

International Journal of Modern Physics: Conference Series
 © World Scientific Publishing Company

Relativistic shock acceleration and some consequences

Martin Lemoine

*Institut d'Astrophysique de Paris, CNRS – UPMC, 98 bis boulevard Arago
 F-75014, Paris, France
 lemoine@iap.fr*

Guy Pelletier

*Institut de Planétologie et Astrophysique de Grenoble, CNRS – UJF, 214 rue de la Piscine
 F-38041 Grenoble Cedex, France
 guy.pelletier@obs.ujf-grenoble.fr*

Received Day Month Year

Revised Day Month Year

This paper summarizes recent progresses in our theoretical understanding of particle acceleration at relativistic shock waves and it discusses two salient consequences: (1) the maximal energy of accelerated particles; (2) the impact of the shock-generated micro-turbulence on the multi-wavelength light curves of gamma-ray burst afterglows.

Keywords: shock waves; particle acceleration; gamma-ray bursts

PACS numbers: 11.25.Hf, 123.1K

1. Introduction

The physics of particle acceleration at relativistic shock waves plays a central role in the modelling of various powerful astrophysical sources, e.g. micro-quasars, pulsar wind nebulae, gamma-ray bursts and active galactic nuclei. In the absence of well motivated prescriptions, it has been customary to adopt phenomenological scalings for the acceleration timescale, such as a Bohm-like $t_{\text{acc}} \simeq \mathcal{A} t_g$ (with t_g the gyro-time, \mathcal{A} a fudge factor) in order to compute quantities of interest, in particular the maximal energy at acceleration.

In the past decades, however, our theoretical understanding of shock physics and shock acceleration has made substantial progress, to the point where one can start to make definite predictions on the inner mechanics of the acceleration process. This contribution to HEPRO-IV summarizes some of these achievements and it discusses some salient consequences for high energy astrophysics.

2. Shock acceleration and micro-physics

A central point in the present discussion is the realization that the development of Fermi-like acceleration at ultra-relativistic collisionless shocks – $\gamma_{\text{sh}}/\beta_{\text{sh}} \gg 1$ with

2 *Martin Lemoine*

$\beta_{\text{sh}} = (1 - 1/\gamma_{\text{sh}}^2)^{1/2}$ the shock velocity in units of c – is intimately connected to the generation of micro-turbulence, on a scale $\lambda_{\delta B} \ll r_g \equiv ct_g$. This has come from different point of views:

- Motivated by the modelling of gamma-ray burst afterglows, which seemingly pointed to the existence of a magnetic field close to equipartition in the shocked region, with $\epsilon_B \sim 10^{-2} - \epsilon_B = \delta B^2 / (16\pi\gamma_{\text{sh}}^2 n_u m_p c^2)$, with n_u the proper density of the unshocked plasma, denotes the equipartition fraction of the turbulent magnetic field downstream of the shock – well above the shock compressed interstellar magnetic field value, Refs. ^{1,2} have proposed that the magnetic field was self-generated in the shock precursor through micro-instabilities, in particular the Weibel/filamentation mode. Such instabilities naturally produce turbulence on microscopic skin depth scales $c/\omega_{\text{pi}} \sim 10^7 n_{u,0} \text{ cm}$ downstream of the shock. Furthermore, for shock heated particles of energy $\epsilon \sim \gamma_{\text{sh}} m_p c^2$, it is easy to see that $r_g \sim \epsilon_B^{-1/2} \lambda_{\delta B} \gtrsim \lambda_{\delta B}$. From the point of view of the accelerated particle population, the turbulence thus lies on small scales.
- Up to ten years ago, most studies of particle acceleration at relativistic shock waves relied on a test-particle picture, in which one treats the shock as a discontinuity and one ignores the back-reaction of the accelerated particles on the shock environment. However, detailed analyses of the particle kinematics, through theoretical arguments ³ and Monte Carlo simulations ⁴, have revealed that the Fermi process can develop only if intense small scale turbulence has been excited on scales smaller than r_g . Otherwise, the particle would be advected with the flow at velocity $c/3$, away from the shock, before it has time to scatter back across the magnetic field; the latter is indeed essentially perpendicular downstream of the shock, due to Lorentz transform and compression effects (i.e. a so-called superluminal configuration ⁵).

As noted in Ref. ³, this argument offers an interesting connection with phenomenology and observations: if the turbulence in gamma-ray burst blast waves is indeed of Weibel/filamentation origin, one has $\lambda_{\delta B} < r_g$ hence this turbulence should provide the requisite conditions for relativistic Fermi acceleration. This point of view has been confirmed by recent particle-in-cell (PIC) simulations, see below.

Further work has pinpointed the requisite characteristics to accelerate particles via the ultra-relativistic Fermi process ^{6,7}: $\lambda_{\delta B} \lesssim r_g \lesssim \lambda_{\delta B} \delta B/B$ with B the background field seen in the downstream rest frame ($B = \sqrt{8}\gamma_{\text{sh}} B_u$ for a perpendicular shock, B_u the upstream-frame field). Note that the r.h.s. imposes an upper bound on the energy of the particle: as energy grows, the scattering frequency in the micro-turbulent field $\nu_s \sim c\lambda_{\delta B}/r_g^2$ becomes less competitive compared to the gyration frequency c/r_g , therefore scattering eventually becomes ineffective and the particle is dragged away from

the shock in the perpendicular magnetic field⁸. One can rewrite the above in terms of the equipartition fraction parameter ϵ_B and the magnetization parameter $\sigma \equiv B_u^2 / (4\pi n_u m_p c^2)$ as follows⁷:

$$\sigma \lesssim \epsilon_B^2, \quad (1)$$

where ϵ_B should be understood in this equation as the average of this value downstream of the shock. Hence, from a purely theoretical analysis of the accelerated particle kinematics, one can predict that acceleration will take place in weakly magnetized shock waves $\sigma \ll 1$. The same arguments teach us that the scattering must take place at a rate $\nu_s \propto \epsilon^{-2}$. As we will see in the following, these scalings have also been confirmed by particle-in-cell (PIC) simulations.

- Finally, the advent of HPC PIC simulations have shown that the micro-turbulence is itself an integral part of the collisionless shock^{9,10,11,12}: micro-instabilities akin to the Weibel/filamentation mode develop in the shock precursor and build-up the micro-turbulence on skin depth scales; this turbulence then grows to a sub-equipartition fraction $\epsilon_B \sim 0.1$ close the shock front, whereby it builds an electromagnetic barrier which isotropizes the incoming background plasma (as seen in the shock front rest-frame), i.e. it initiates the shock transition.

The three above point of views meet and complement each other, underlying the intimate non-linear relationship between shock structure, micro-instabilities and particle acceleration.

The simulations of Ref.¹³ have made another step forward, in demonstrating that in the unmagnetized limit $\sigma \rightarrow 0$, the self-generated micro-turbulence provides the source of scattering that leads to the development of the Fermi process. The number of PIC simulations of shock acceleration has then kept growing, in order to probe in which conditions of magnetization and shock velocity acceleration takes place and at what rate; such progresses are related in the contribution of L. Sironi in this volume. These simulations confirm the predictions of the theoretical analyses described above: in particular, Fermi acceleration is seen to take place at low magnetization $\sigma \lesssim 10^{-5}$, as expected from Eq. 1, with a rate of order ν_s , also as expected.

Naturally, the study of micro-instabilities upstream of shock fronts has received ample attention, in particular the dominant Weibel/filamentation mode^{2,14,15,16,17,18,7,19,20,21} at low magnetization levels. The comparison of the growth rate of this instability, $\Im\omega \sim \xi_{cr}^{1/2}\omega_{pi}$ (with $\xi_{cr} \sim 0.1$ the fraction of incoming energy transferred to the accelerated particle population) with the rate at which the background plasma crosses the shock precursor, $t_x^{-1} \sim \sigma^{1/2}\gamma_{sh}\omega_{pi}$, limits the parameter space in which this instability actually has time to grow and build up the micro-turbulence⁷:

$$\sigma \lesssim \gamma_{sh}^{-2}\xi_{cr}. \quad (2)$$

Whenever this bound is not satisfied, the Weibel/filamentation instability cannot structure the shock by itself. As discussed by G. Pelletier in this volume, the relevant instability over all remaining parameter space, is a current-driven instability which can develop for any value of the shock Lorentz factor, provided $\sigma \lesssim 10^{-2}$. This instability also produces micro-turbulence on a skin depth scale, therefore the results that follow apply to this case as well. Above 10^{-2} in magnetization, the shock can be mediated by the direct compression of the magnetic field and by the development of the synchrotron-maser instability ²².

In spite of these successes, one must keep in mind the rather large number of open questions in this field, as well as the gap which remains between the timescales probed by the PIC simulations and the astrophysical timescales. So far, the longest PIC simulation ²³ has run over $\sim 10^4 \omega_p^{-1}$ for a pair shock, which represents a fraction of a percent of the dynamical timescale of a gamma-ray burst in the early afterglow phase. Theoretical extrapolation is thus needed to connect these simulations to actual sources. Finally, as emphasized in Ref. ²³, PIC simulations have not yet converged to a stationary state and the acceleration of particles to progressively higher energies appears to feed back on the shock structure as time goes on. With these caveats in mind, we now discuss two macrophysical consequences of this microphysics of relativistic shock acceleration.

3. Acceleration to very high energies

Formally, the acceleration timescale in the shock frame reads: $t_{\text{acc}} \simeq (t_{\text{d|sh}} + t_{\text{u|sh}})/2$, with $t_{\text{d|sh}}$ (resp. $t_{\text{u|sh}}$) the downstream (resp. upstream) residence time expressed in the shock frame; the factor 2 corresponds to the typical energy gain per cycle ^{24,25}. These residence times depend inversely on the scattering frequency, which in turn is controlled by the scale, the velocity and geometry of the micro-turbulence, as discussed in detail in ^{8,26}. In particular, scattering in the shock precursor may be hampered by the anisotropic nature of the turbulence, since the near independence of turbulent modes along a given direction implies the conservation of the conjugate momentum ²⁷. In such cases, the scattering may be controlled by the background magnetic field upstream of the shock, but by the micro-turbulence downstream of the shock, which appears essentially isotropic and static there ^{28,23}.

3.1. *Electrons*

To simplify the discussion, one may assume that scattering takes place in the micro-turbulence at a rate $\nu_s \simeq c\lambda_{\text{dB}}/r_g^2$ on both sides of the shock. Then, balancing $t_{\text{acc}} \sim \nu_s^{-1}$ with the timescale for synchrotron losses allows to compute the maximal Lorentz factor of shock-accelerated electrons ²⁹:

$$\gamma_{e,\text{max}} \simeq (r_e^3 n_u m_e / m_p)^{-1/6} \simeq 7 \times 10^6 n_{u,0}^{-1/6}, \quad (3)$$

in terms of the classical electron radius r_e , assuming here $\lambda_{\delta B} \simeq c/\omega_p$. This gives rise to synchrotron photons of maximal energy

$$\epsilon_{\gamma, \max} \simeq 3 \text{ GeV } \epsilon_{B,-2}^{1/2} \gamma_{\text{sh},2.5}^2 n_{\text{u},0}^{1/2}. \quad (4)$$

In order to draw comparison with actual observations of gamma-ray burst afterglows, one needs to take into account the temporal dependence of the shock Lorentz factor through the deceleration phase; the above maximal energy then corresponds to an observer timescale $t_{\text{obs}} \sim 100 \text{ s}$ for an isotropic shock energy 10^{54} ergs ; beyond this timescale, it decays as $t_{\text{obs},2}^{-\alpha_\epsilon}$, with $\alpha_\epsilon \simeq 2/3 \rightarrow 3/4$ depending on the external density profile, see 30,31,32.

The *Fermi-LAT* instrument has detected extended emission $> 100 \text{ MeV}$ well beyond the prompt duration phase in a subset of gamma-ray bursts; at high energies, the spectral power appears to follow the scaling $F_\nu \propto \nu^{-\alpha} t_{\text{obs}}^{-\beta}$ with $\alpha \sim 1$ and $\beta \sim 1$, as expected for the synchrotron contribution of an electron spectrum $dn_e/d\gamma_e \propto \gamma_e^{-s}$ with $s \simeq 2.2$. Very few photons have been collected with source rest-frame energies $> 10 \text{ GeV}$, therefore it is not yet possible to constrain the maximal energy at acceleration from observations. The above discussion rather suggests that those photons seen above 10 GeV are most likely of inverse Compton origin³². Interestingly, the recent GRB 130427A has been observed with unprecedented detail at high energies, on timescales as large as 10^5 s . The spectrum of the extended emission for this burst reveals a clear distinct component above a few GeV, which is well reproduced by a synchrotron-self-Compton component^{33,34}. The light curve and the spectrum of this gamma-ray burst thus conform rather well to the above expectations.

3.2. Protons

One can also compute the maximum energy of protons accelerated at the external shock wave, by balancing the acceleration timescale with the dynamical timescale. One then finds maximal energies of order 10^{16} eV , the exact prefactor depending on whether one assumes that scattering is dominated by the small-scale field or by the large scale field upstream of the shock^{35,36,37,26}. Among others, this confirms that the external shock wave of gamma-ray bursts cannot produce particles in the ultra-high energy range.

The difficulty of pushing particles to extreme energies in ultra-relativistic shock waves is directly associated to the small-scale nature of the turbulence and the associated energy scaling of the scattering rate, which implies $t_{\text{acc}} \propto t_g r_g / \lambda_{\delta B} \gg t_g$. Invoking a large external magnetic field would not help, because the dynamic range $\gamma_{\text{max}}/\gamma_{\text{min}}$ available to acceleration scales at most as $\delta B/B \sim (\epsilon_B/\sigma)^{1/2}$, see the discussion around Eq. (1).

There are nevertheless loopholes in the above argument, which may lead to potential acceleration sites of ultra-high energy cosmic rays. First of all, the above discussion applies to ultra-relativistic shock waves; for mildly relativistic shock waves,

$\gamma_{\text{sh}}\beta_{\text{sh}} \sim \mathcal{O}(1)$, the shock may be sub-luminal in a substantial part of parameter space, hence Eq. (1) does not necessarily hold. This suggests that acceleration might take place in large-scale, possibly self-amplified, turbulence, with a fast scattering closer to the Bohm limit at high energies. Acceleration to ultra-high energies at such shock waves has been proposed in gamma-ray bursts ^{38,39}, blazars ⁴⁰ and in trans-relativistic supernovae ^{41,42,43,44}, although the latter could push only heavy nuclei up to 10^{20} eV. Another loop-hole is the implicit assumption of a steady planar shock front; if an additional source of turbulence or dissipation exists in the vicinity of the shock, then one might circumvent the limitation of ultra-relativistic acceleration. The termination shock of the wind of the Crab pulsar, and other pulsar wind nebulae, provides a nice example: with a shock magnetization $\sigma \gtrsim 10^{-2}$ and shock Lorentz factor $\gamma_{\text{sh}} \sim 10^3 - 10^6$, the Crab unexpectedly accelerates electrons at a Bohm-like rate, up to PeV energies; yet, how acceleration takes place in such objects remains a subject of debate, see Ref. ⁴⁵ for a detailed discussion. One should thus question whether the termination shocks of young pulsar winds, if they output ions, could not accelerate such particles to ultra-high energies; work is in progress and preliminary results are encouraging.

4. Synchrotron spectra in micro-turbulence

The small-scale nature of the turbulence is also likely to entail departures from the standard synchrotron spectra of relativistic blast waves. The possibility of a diffusive synchrotron regime, in which the electron wanders over several coherence cells of the magnetic field while the emission cone of aperture $\sim 1/\gamma_e$ sweeps the line of sight, has received much attention, e.g. ^{46,47,29,48,49,50}. However it is now recognized that such effects must remain very limited at relativistic shock waves because the wiggler parameter $a \equiv e\delta B\lambda_{\delta B}/(m_e c^2) \sim \gamma_{\text{min}}\epsilon_{B,-2}^{1/2}$ with $\gamma_{\text{min}} \sim \gamma_{\text{sh}} m_p/m_e \gg 1$ the typical Lorentz factor of the accelerated electrons; $a \gg 1$ means that the spectral power emitted follows closely the standard synchrotron shape.

Nevertheless, the turbulence is expected to decay on short timescales through phase mixing ¹ and PIC simulations do confirm this decay with a rough behavior $\epsilon_B \propto t^{\alpha_t}$, $\alpha_t \sim -0.5$ ^{28,23}, see also the discussion in Ref. ³⁰; in this equation, t designs the time of injection of the plasma element through the shock, in the comoving downstream frame; thus, $t \sim 3\Delta x/c$ where Δx is the distance to the shock front. This decay implies that along its cooling history, an electron will cool in a magnetic field of decreasing strength, which directly modifies the synchrotron spectral power of a single electron. Furthermore, electrons of different Lorentz factors cool in regions of different magnetic field strengths due to the energy dependence of the cooling time. This has obvious consequences for the synchrotron spectrum of a relativistic blast wave. The departures from the standard one-zone synchrotron spectrum have been addressed in simplified limits in Refs. ^{51,52} and calculated in detail in Ref. ³⁰, which has also quantified the impact on the light curve of a decelerating blast wave. Figure 1 illustrates this departure by comparing the synchrotron spectrum of a

gamma-ray burst in the homogeneous model with $\epsilon_B = 0.01$ (upper red curve) and in a model with power-law decaying microturbulence, $\epsilon_B = 0.01 (t/100\omega_p^{-1})^{-0.8}$ (lower blue curve) assuming in both cases that inverse Compton losses dominate the cooling history with $Y = 3$ for the Compton parameter close to the shock front.

In this frame, it is interesting to note that the synchrotron modeling of the extended high energy emission seen by the *Fermi-LAT* instrument in several gamma-ray bursts systematically point to quite low values $\epsilon \sim 10^{-6} - 10^{-4}$ 53,54,55,56,44. As discussed in Ref. 30, such values may actually attest of the decay of the turbulence downstream of the shock; this would allow to reconcile the afterglow models of gamma-ray bursts with the predictions of PIC simulations, a long-standing problem in this field. As an order of magnitude estimate, note that the blast width is typically 10^7 skin depths c/ω_p , so that the power-law decay of ϵ_B down to $\sim 10^{-5}$, starting at 0.01 some $100c/\omega_p$ away from the shock, indeed takes place on the scale of the blast if $\alpha_t \sim -0.5$.

More quantitatively, one can build an approximate two-zone model of the blast: a first zone close to the shock front with $\epsilon_{B,+} \sim 0.01$, in which the highest energy electrons cool and produce the > 100 MeV emission; a second zone with $\epsilon_{B,-} \ll \epsilon_{B,+}$, close to the contact discontinuity, where electrons, which do not cool on a dynamical timescale, output most of their synchrotron emission. This latter region produces the low energy part of the synchrotron spectrum, i.e. the radio, optical and at early times the X-ray region. One can use the standard homogeneous synchrotron model

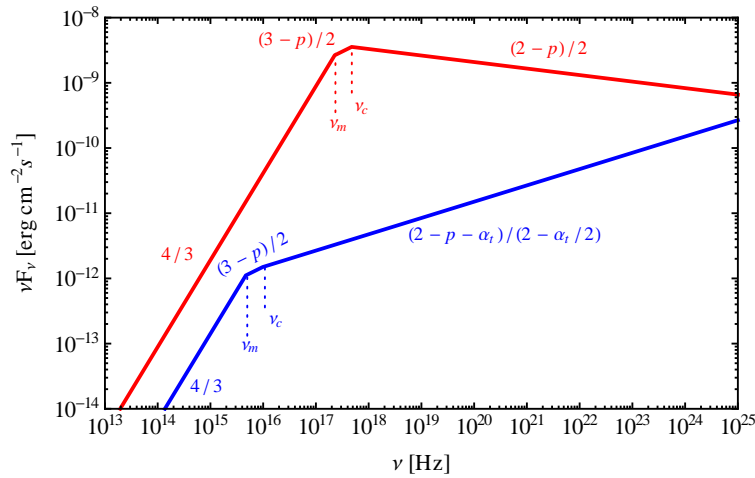


Fig. 1. Comparison of the synchrotron spectrum in a homogeneous turbulence of strength $\epsilon_B = 10^{-2}$ (upper red curve) with a decaying microturbulence such that $\alpha_t = -0.8$ (lower blue curve), assuming in both cases dominant inverse Compton energy losses with $Y = 3$. This case assumes $\gamma_b = 245$, $n = 0.001 \text{ cm}^{-3}$, an injection distribution index $p = 2.2$, and a cooling time of the electrons longer than the dynamical timescale.

for each zone and adjust the model to the data to derive $\epsilon_{B,-}$. This reconstruction is discussed in detail in Ref. ⁵⁷. A non-trivial aspect is the fact that the low-energy electrons cool mostly through inverse Compton interactions, due to the low value of $\epsilon_{B,-}$ and, in the case of X-ray emitting electrons, Klein-Nishina suppression of the inverse Compton interactions is significant. The cooling history of these electrons is thus not trivial and this effect needs to be taken into account, otherwise incorrect values for the microphysical parameters would be derived from the observations. Furthermore, the afterglow model depends on 4 main parameters: 2 macrophysical (blast energy E and external density n) and 2 microphysical ($\epsilon_{B,-}$ and $\epsilon_e \sim 0.1$); the parameters p and k , which characterize respectively the injection spectral index and the circumburst density profile, can be derived from the slopes of the light curve. In order to derive the 4 parameters, one thus needs to adjust the model to 4 different wavebands. For this reason, Ref. ⁵⁷ has studied gamma-ray bursts afterglows that were caught in the radio, optical, X-ray and at high energy > 100 MeV. Once such a proper reconstruction of $\epsilon_{B,-}$ is carried out, one finds quite remarkably, a coherent value of the decay exponent α_t among the four bursts studied, $-0.5 \lesssim \alpha_t \lesssim -0.4$. Whether this result pertains over a larger number of gamma-ray bursts remains to be seen, of course. It is interesting to note that the recent GRB 130427 fits well in this model, because its modelling leads to $\alpha_t \simeq -0.45$. At the very least, these results raise the exciting prospect of probing the physics of shock-generated Weibel turbulence through the multi-wavelength afterglows of gamma-ray bursts.

5. Summary

This paper summarizes recent progresses in our theoretical understanding of particle acceleration at relativistic shock waves. Emphasis is placed here on the intimate relationship that appears to tie the generation of micro-turbulence in the precursor of ultra-relativistic shock waves ($\gamma_{\text{sh}} \gg 1$) and the efficiency of particle acceleration. The arguments reported here have been developed at an analytical level and validated by particle-in-cell simulations. This includes in particular the development of acceleration over a broad dynamic range whenever the magnetization of the upstream plasma ⁷ $\sigma \lesssim \epsilon_B^2 \sim 10^{-5}$, assuming micro-turbulence has been excited by Weibel/filamentation or through a current instability discussed by G. Pelletier in this volume.

This paper then discusses two salient consequences of this micro-turbulence: (1) the maximal energy of particle accelerated at the shock, which departs from the Bohm scaling because the scattering frequency in the micro-turbulence decreases with increasing energy; (2) the impact of the evanescent nature of this micro-turbulence on the afterglow spectra and light curves of gamma-ray bursts, where it is argued in particular that the decay of this turbulence may well have been indirectly observed in gamma-ray bursts with extended high energy emission.

References

1. Gruzinov, A., Waxman, E., *ApJ* **511**, 852 (1999).
2. Medvedev, M. V., Loeb, A., *ApJ* **526**, 697 (1999).
3. Lemoine, M., Pelletier, G., Revenu, B., *ApJ* **645**, L129 (2006).
4. Niemiec, J., Ostrowski, M., Pohl, M., *ApJ* **650**, 1020 (2006).
5. Begelman, M. C., Kirk, J. G., *ApJ* **353**, 66 (1990).
6. Pelletier, G., Lemoine, M., Marcowith, A., *MNRAS* **393**, 587 (2009).
7. Lemoine, M., Pelletier, G., *MNRAS* **402**, 321 (2010).
8. Plotnikov, I., Pelletier, G., Lemoine, M., *A&A* **532**, 68 (2011).
9. Spitkovsky, A., *AIPC* **810**, 345 (2005).
10. Kato, T., *ApJ* **668**, 974 (2007).
11. Spitkovsky, A., *ApJ* **673**, L39 (2008).
12. Nishikawa, K.-I., Niemiec, J., Hardee, P. E., Medvedev, M., Sol, H., Mizuno, Y., Zhang, B., Pohl, M., Oka, M., Hartmann, D. H., *ApJ* **698**, L10 (2009).
13. Spitkovsky, A., *ApJ* **682**, L5 (2008).
14. Wiersma, J., Achterberg, A., *A&A* **428**, 365 (2004).
15. Lyubarsky, Y., Eichler, D., *ApJ* **647**, L1250 (2006).
16. Achterberg, A., Wiersma, J., *A&A* **475**, 19 (2007).
17. Achterberg, A., Wiersma, J., Norman, C. A., *A&A* **475**, 1 (2007).
18. Bret, A., Gremillet, L., Bénisti, D., *Phys. Rev. E* **81**, 036402 (2010).
19. Lemoine, M., Pelletier, G., 2011, *MNRAS* **417**, 1148
20. Rabinak, I., Katz, B., Waxman, E., *ApJ* **736**, 157 (2011).
21. Shaisultanov R., Lyubarsky Y., Eichler D., *ApJ* **744**, 182 (2012).
22. Alsop, D., Arons, J., *Phys. Fluids* **31**, 839 (1988).
23. Keshet, U., Katz, B., Spitkovsky, A., Waxman E., *ApJ* **693**, L127 (2009).
24. Achterberg, A., Gallant, Y., Kirk, J. G., Guthmann, A. W., *MNRAS* **328**, 393 (2001).
25. Lemoine, M., Pelletier, G., *ApJ* **589**, L73 (2003).
26. Plotnikov, I., Pelletier, G., Lemoine, M., *MNRAS* **430**, 1280 (2013).
27. Jones, F. C., Jokipii, J. R., Baring, M. C., *ApJ* **509**, 238 (1998).
28. Chang, P., Spitkovsky, A., Arons, J., *ApJ* **674**, 378 (2008).
29. Kirk, J. G., Reville, B., *ApJ* **710**, 16 (2010).
30. Lemoine, M., *MNRAS* **428**, 845 (2013).
31. Sironi, L., Spitkovski, A., Arons, J., *ApJ* **771**, 54 (2013).
32. Wang, X.-Y., Liu, R., Lemoine, M., *ApJ* **771**, L33 (2013).
33. Tam, P.-H. T., Tang, Q.-W., Hou, S., Liu, R.-Y., Wang, X.-Y., *ApJ* **771**, L13 (2013).
34. Liu, R.-Y., Wang, X.-Y., Wu, X.-F., *ApJ* **773**, L20 (2013).
35. Gallant, Y., Achterberg, A., *MNRAS* **305**, L6 (1999).
36. Eichler, D., Pohl, M., *ApJ* **738**, L21 (2011).
37. Bykov, A., Gehrels, N., Krawczynski, H., Lemoine, M., Pelletier, G., Pohl, M., *Sp. Sc. Rev.* **173**, 309 (2012).
38. Waxman, E., *PRL* **75** 386 (1995).
39. Gialis, D., Pelletier, G., *A&A* **425**, 395 (2004).
40. Dermer, C., Razzaque, S., Finke, J. D., Atoyan, A., *New J. Phys.* **11**, 5016 (2009).
41. Wang, X.-Y., Razzaque, S., Mészáros, P., Dai, Z.-G., *PRD* **76**, 083009 (2007).
42. Budnik, R., Katz, B., MacFadyen, A., Waxman E., *ApJ* **673**, 928 (2008).
43. Chakraborti, S., Ray, A., Soderberg, A. M., Loeb, A., & Chandra, P., *Nature Comm.*, **2** (2011).
44. Liu, R.-Y., Wang, X.-Y., *ApJ* **746**, 40 (2012).
45. Kirk, J. G., Lyubarsky, Y., Pétri, J., *ASSL* **357**, 421 (2009).
46. Medvedev, M. V., *ApJ* **540**, 704 (2000).

47. Fleishman, G. D., Urtiev, F. A., *MNRAS* **406**, 644 (2010).
48. Mao, J., Wang, J., *ApJ* **731**, 26 (2011).
49. Medvedev, M. V., Trier Frederiksen, J., Haugboelle, T., Nordlund, A., *ApJ* **737**, 55 (2011).
50. Kelner, S. R., Aharonian, F. A., Khangulyan, D., *ApJ* **774**, 61 (2013).
51. Rossi, E., Rees, M. J., *MNRAS* **339**, 881 (2003).
52. Derishev, E., *Astrophys. Sp. Sc.* **309**, 157 (2007).
53. Kumar, P., Barniol-Duran, R., *MNRAS* **400**, L75 (2009).
54. Kumar, P., Barniol-Duran, R., *MNRAS* **409**, 226 (2010).
55. Barniol-Duran, R., Kumar, P., *MNRAS* **412**, 522 (2011).
56. He, H.-N., Wu, X.-F., Toma, K., Wang, X.-Y., Mészáros, P., *ApJ* **733**, 22 (2011).
57. Lemoine, M., Li, Z., Wang, X.-Y., *MNRAS* **435**, 3009 (2013).